Preservation of Cultural Heritage: A Comparison Study of 3D Modelling between Laser Scanning, Depth Image, and Photogrammetry Methods

.

Mohamad Haziq Ahmad Yusri,
Centre of Postgraduate Studies, Universiti Teknologi MARA, Selangor, Malaysia

M. A. Johan
School of Mechanical Engineering, College of Engineering, Universiti Teknologi MARA, Terengganu, Malaysia

N. S. Khusaini, M. H. M. Ramli[*]
Sports Engineering and Artificial Intelligence, College of Engineering, Universiti Teknologi MARA, Selangor, Malaysia
[*]haniframli@uitm.edu.my

ABSTRACT

This paper presents a multi-technique approach for the purpose of recording and documentation of cultural heritage. The focal point of the study is to generate a three-dimensional (3D) model representation of a physical object and to apply orthographic projection to document the design. Three main methods are used to generate 3D objects, namely Laser Range Scanner, Depth Image Data, and Photogrammetry. A comparison analysis is designed to evaluate each method accordingly. For evaluation purposes, a case study is designed where a scale model of a 25-cm-long famous historic Portuguese Indian Armada, known as "Flor de la Mar" is selected as a sample for generating 3D model records. The comparison analysis shows that the Photogrammetry method is superior in terms of detail, precision, and visualization. On the other hand, Laser Range Scanner and Depth Image Data method can display the data into the point cloud but with less accuracy. Overall, the result shows that the Photogrammetry method achieves a strong 97.6% of accuracy in terms of dimensions and shapes.

ISSN 1823-5514, eISSN 2550-164X

Received for review: 2021-06-06
Accepted for publication: 2022-03-09
Published: 2022-04-15

Keywords: *Photogrammetry; 3D Model; Laser Scanning; Heritage Preservation; Depth Image*

Introduction

Traditional sailing vessels are unique, and it is a part of the Terengganu cultural heritage. The vessels must be conserved in order to preserve the state's, country's, and indigenous people's talents in Malaysia. Traditional sailing vessels give important contributions to present and future generations due to their unique method of architectural and sculptural carving elements. These characteristics reflect previous generations' dominance in the marine sector. This is due to the fact that water transport is one of the features in Malay-Polynesian culture. Their knowledge in sailing and oceanography permits them to travel and be scattered all over the world. However, the sailing vessel's artisans do not have any document about the schematic design or what can be called as 'blueprint' in representing the traditional sailing vessels. They sketch and plan the design on a piece of wood and walls in an irregular state. So, it is impossible to collect and record the design precisely. It is a loss if the knowledge of this precious heritage is buried within the artisans themselves. Therefore, there is clearly a need to preserve traditional sailing vessels. As of present, manual hands-on measurement of structural elements such as Laser Measuring Tool (LMT) and Measuring Tape (MT) are commonly used.

Obtaining geometric information from conventional sailing vessels by hands-on measurement, on the other hand, takes a long time and might be dangerous if done from a higher vantage point. Furthermore, due to the enormous size of a conventional sailing vessel, measuring the mast height from the vessel's deck is challenging; additionally, some of the targeted structural elements are blocked by another structural element nearby. This study considers three potential techniques to overcome the limitations of traditional methodologies.

The first method is by using a Laser Range Scanner called Light Detection and Ranging (LiDAR) sensor that uses light in the form of a pulsed laser to measure distance. Over the past years, LiDAR has been used in the robotics sector to avoid obstacles within a pre-determined range. Linghui Sui et al. [1] design an autonomous household cleaning robot using low-cost 2D LiDAR in a Robot Operating System (ROS) environment. The LiDAR collects surrounding data while the cleaning robot moves throughout the entire room and later constructs a two-dimensional (2D) map. Interestingly, LiDAR is also capable of creating a three-dimensional (3D) mapping by making fine adjustments to the 2D model. For instance, Pena Queralta et al. [2] used multiple rotating 2D LiDARs to produce a 3D world visualization using ROS environment while Nicolás Llanos Neuta et al. [3] developed a 3D perception system robot using a single 2D LiDAR.

Depth Image is the second method employed in this investigation. Kinect sensor technology is improving and advancing in order to apply the concept of depth imaging to customers. An RGB camera, a depth sensor, and four microphone arrays are among Kinect's advanced motion capture capabilities, which help it recognise a user's facial features and movements. The Kinect camera collects colour and 3D depth photographs at 30 frames per second, resulting in a cloud of colour and depth images based on an infrared pattern on the scene. It can scan both human motion and depth images. Ratha Siv et al. [4] used Kinect Version 2 to rebuild a 3D human face and applied the Poisson surface approach to reduce noise. The scanning region focuses primarily on the subject's face, and the distance between the Kinect's console and the person is designated between 500 mm and 700 mm. When the Poisson surface method is employed, the outcome shows a smoother surface of the 3D reconstructed face when compared to the surface generated without the Poisson method.

The final technique entails the use of Photogrammetry to create a 3D model for measuring the dimensional specifications of traditional sailing vessels. Fabrizio Ivan Apollonio et al. [5] constructed a 3D visualization of museum's assets using photogrammetry-based workflow. A combo of acquisition, based on mobile gear and real-time rendering was proposed. Calibration was performed utilizing two distinct devices and four different targets to perform photogrammetry. The iPhone X and Nikon DS200 were utilized in this experiment. The quality and correctness of four distinct pieces were examined: Marsili Bust, Heracles, Horn d'Arturo's Globe, and Porcupine Fish Artifacts. iPhone X's (smartphone camera) photographic results meet the industry standard of excellent quality inside a streamlined photogrammetric workflow, which are virtually equivalent to the Nikon DS200 (SLR camera).

Based on the findings of prior research, these techniques had a good probability of functioning effectively for scanning a particular object. However, since dependable and accurate scanning methods are not yet available, the use of those methods for scanning a specific object is still in the experimental stages [1][2][4][5].

The goal of this research is to create a standard sailing vessel orthographic projection that may be used as a template for other projects. The initial part of the inquiry was to try out all three scanning technologies to see which one worked best for scanning vintage sailing vessels. In order to make a basis of measurement, an actual case study is devised, and in this study, a 25-cm-long wooden replica of the famed Portuguese Indian Armada, the "Flor de la Mar" is utilised as a sample. Using previous processes, the rest of the investigation was carried out to get precise structural member measurements. Using the 3D Modeler programme, the classic sailing sailboat was projected from digital 3D model data.

3D Scanning Methods

Laser scanning

Time-of-flight (ToF) scanning utilizes a ToF concept in getting distance measurements of an object. The laser-based method employs a laser beam to demonstrate how pulses of light travel and return to their origin. This answers the question of how far away the object is.

The traditional sailing sailboat in the experiment is scanned using an RPLiDAR A2M8 LiDAR sensor. According to an investigation done by Xueyang Kang et al. [6], an RPLiDAR A2M8 is considered acceptable for three-dimensional mapping reconstruction. This LiDAR delivers adequate performance for indoor application within a range of 16 meters and 8000 samples per second. The proposed scanning system is depicted in Figures 1 and 2. The 3D scanner includes a stepper motor and controller, as well as a LiDAR sensor and two microcontrollers. The main control board for the scanner is a Raspberry Pi 4B, which runs the Robotic Operating System (ROS) for hosting 3D visualisation programmes. The Arduino Uno, on the other hand, oversees the stepper motor's movement (microcontroller board). The back-and-forth movement of a stepper motor is seen in three dimensions in Figure 3.

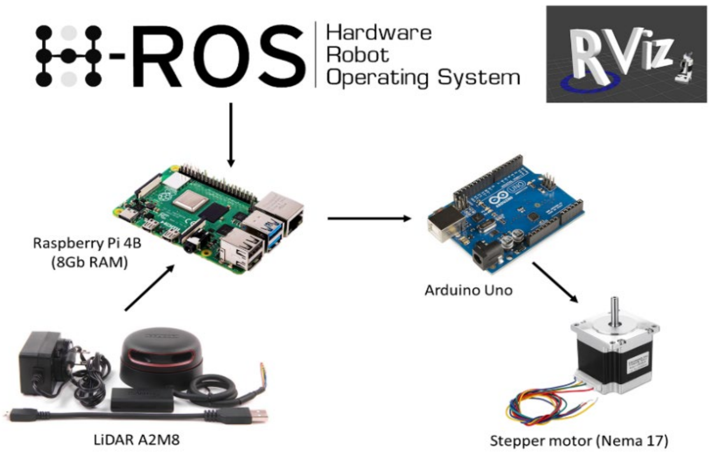

Figure 1: The components used for laser scanning method

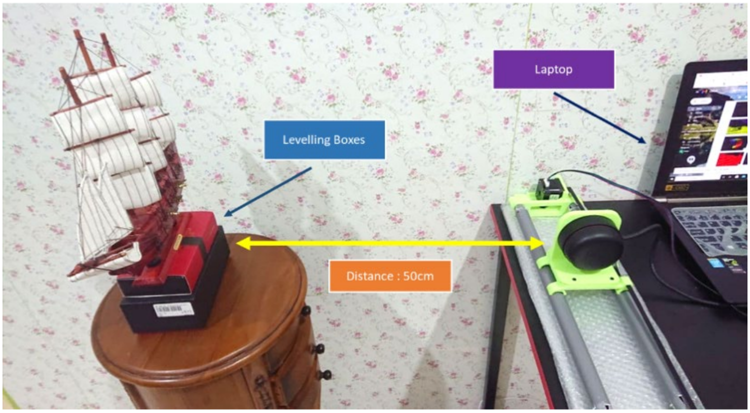

Figure 2: The proposed laser-based scanner setup

This method also was inspired by Pena Queralta et al. [2]; where three mounted LiDARs are used to obtain a 3D visualization of a designated room. Similarly, Shahrin et al. [7] generated a 3D map using an inexpensive 2D LiDAR sensor controlled by an Arduino Uno and moved by two servos. Instead of servos, the researchers use a stepper motor to boost scanning and plotting precision.

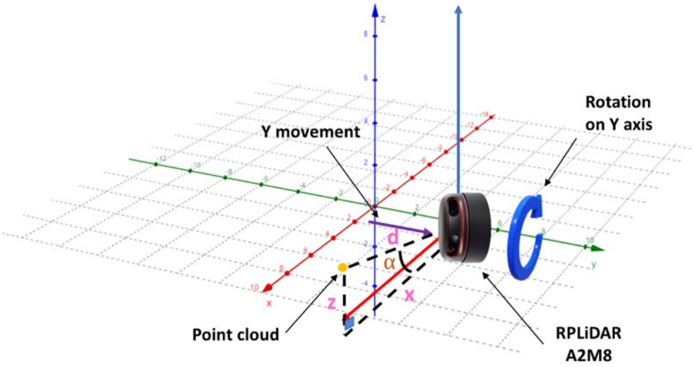

Figure 3: 3D space point cloud plot by the laser scanner

The Raspberry Pi 4B runs Ubuntu alongside the ROS Kinetic framework, giving it an excellent platform for 3D graphing scanned data with the ROS Visualization (RVIZ) plugin. The data in a 3D cartesian plane is plotted using Equation (1)-(3).

$$x = \cos \alpha \, . \, d \qquad (1)$$

$$y = linear\ incremental\ by\ 5\ mm \tag{2}$$

$$z = \sin \alpha \,.\, d \tag{3}$$

On RVIZ, Jing Li et al. [8] and Juan Li et al. [9] developed a 3D semantic map building utilising a combination of LiDAR and camera vision. They improved the data by combining each of them into a single point cloud, which resulted in increased accuracy and visibility over a larger scanning region. The LiDAR sensor and camera were tested individually for this study. The laser scanning procedure is depicted in Figure 4 as a flow chart.

Depth camera scanning

A depth camera often referred to as a multi-resolution active 3D imaging sensor, is capable of creating dozens of photos with depth information each second [10]. Like laser scanning, the ToF principle of structured light is also used in-depth cameras to provide a 3D image. Because it combines the technologies of RGB-D cameras, infrared projectors, and detectors that map depth through ToF at a low cost, Microsoft Kinect has stimulated a lot of research [11]. Kinect was immediately accepted by researchers to learn more about the 3D data range used in creating virtual worlds. By object recognition method, some researchers utilise it to distinguish between living and non-living items [12].

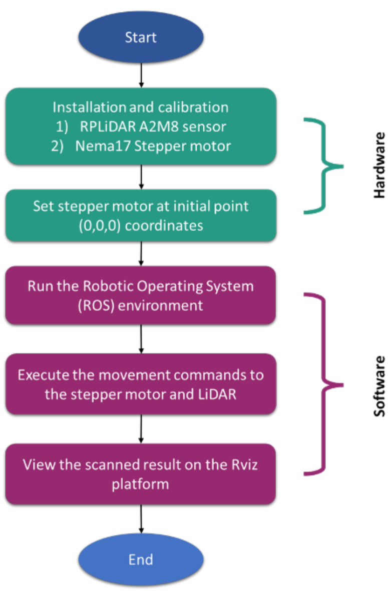

Figure 4: Laser scan process flow-chart

The Kinect V2 is used in this study to perform 3D scanning experiments to assess the usability and quality of the 3D scanning data. Kinects are available in two versions: Kinect V1 and Kinect V2. The Kinect V1 can shoot 30 frames per second (fps) with its 320x240 camera, and its maximum depth distance is 4.5 meters. The Kinect V2 has a new camera with a resolution of 512x424 at 30 frames per second (fps) and a maximum depth of 5.5 meters. According to Samir et al. [13], the Kinect V2 outperforms the Kinect V1. As a result, the Kinect V2 was chosen for this case study.

The overall process flow is shown in Figure 5. The procedure begins with the installation and calibration of Kinect V2 using the Software Development Kit that is provided (SDK). The scanning procedure will then commence with the global coordinate system being initialised. During the first scanning operation, the Kinect V2 will automatically set its coordinate system to the origin in three dimensions while simultaneously acquiring a depth image of the environment. The Poisson surface approach is then used to recreate a classic sailing vessel, as demonstrated by Ratha Siv et al. [4]. Following the scanning technique, 3D point cloud data is produced and converted to the OBJ format for further processing and manipulation. At the end of the procedure, the OBJ data is processed using meshing software such as MeshLab to smooth and harden the surface area of the 3D scanned item.

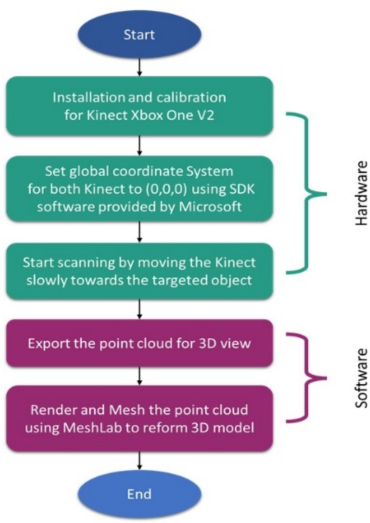

Figure 5: 3D scanning flowchart for depth camera

Photogrammetry

Digital photogrammetry is a technique for creating a three-dimensional (3D) model of an object by overlapping two-dimensional (2D) images collected while measuring the size, shape, and 3D geometric location of the object. The allocated location on the pictures is used as the basis for the operation's principle of operation. There must be at least two images in the points connection that can be used to generate the 3D object coordinates. Increasing the number of intersections between assigned points in a 3D model could increase the overall quality of the model. The above-mentioned process is proven to be effective as seen in [14] and [15].

It is important to note that the camera location has a considerable impact on the production of the 3D model, with the position of the camera being determined by the size and shape of the object, as shown in [16]. Aside from that, selecting a different sort of camera results in a distinct 3D model because each camera has dedicated pixels and a fixed focal length, which is occasionally changeable.

This project uses an Honor 9 Lite with a 2 MP camera with a depth sensor and a 26mm focal length to capture photographs and create 3D models using Structure-from-Motion (SFM)-based software. The phone contains a depth sensor with a focal length of 26mm. Figure 6 depicts the overall process flow. The procedure is straightforward because the SFM programme handles most of the processing and rendering tasks, including calculating the point localization for each image, image orientation, depth images, and blur photos filtering, and eventually creating a precise 3D model. In order to create a 3D model with a smooth surface, the lighting must be carefully regulated when the photographs are being taken [17].

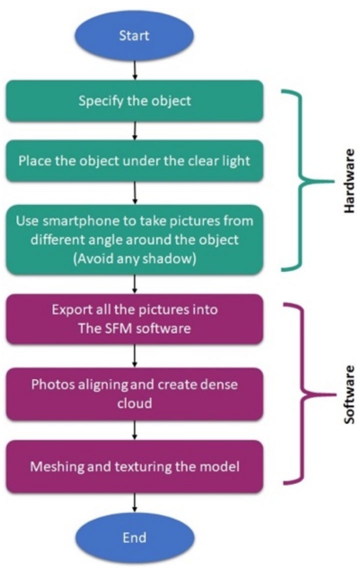

Figure 6: 3D modelling process using photogrammetry method

During the photography task, the camera is set to a constant focal length i.e., without zooming as illustrated in Figure 7 and Figure 8. The first image is captured from the perpendicular direction of the object and denoted as *k^th^* position. The following position is *k+1^th^* until *k+n^th^*, with *n* is the total number of images required to generate the 3D model. The camera position and orientation can be calculated by using Equations (4)-(9) as demonstrated in [18]. A further illustration of the changes with respect to coordinate and orientation from position *k^th^* to *k+1^th^* is depicted in Figure 9. Linear position in (X, Y, Z) coordinate:

$$X_{k+1} = X_k + (R_{lx} - P_{lx}) \tag{4}$$

$$Y_{k+1} = Y_k + (R_{ly} - P_{ly}) \tag{5}$$

$$Z_{k+1} = Z_k + (R_{lz} - P_{lz}) \tag{6}$$

Angular position in $(\theta_x, \theta_y, \theta_z)$:

$$\theta_{(k+1),x-axis} = \theta_{(k),x-axis} + \theta_x \tag{7}$$

$$\theta_{(k+1),y-axis} = \theta_{(k),y-axis} + \theta_y \tag{8}$$

$$\theta_{(k+1),z-axis} = \theta_{(k),z-axis} + \theta_z \tag{9}$$

where R_{lx}, P_{lx} is the base length (*m*) at k^{th} and $k+1^{th}$ position respectively, R_{ly}, P_{ly} is the Mainmast height (m) at k^{th} and $k+1^{th}$ position respectively, R_{lz}, P_{lz} is the Base depth (*m*) at k^{th} and $k+1^{th}$ position respectively, θ_x is the angle differences between R_{lx} and P_{lx},while θ_y, is the angle difference between R_{ly} and P_{ly}, and lastly θ_z is the angle difference between R_{lz}, and P_{lz}.

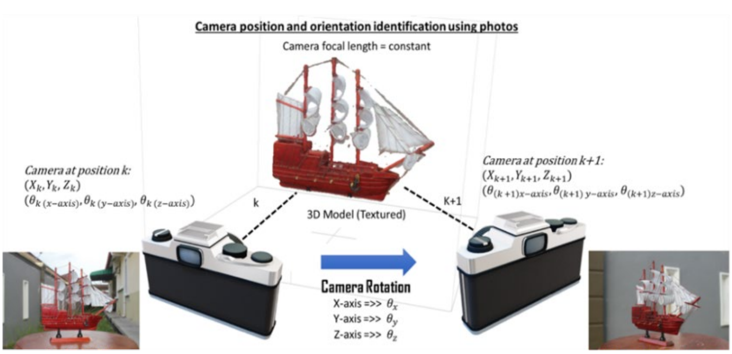

Figure 7: Illustration of photography scene at different angles and orientation

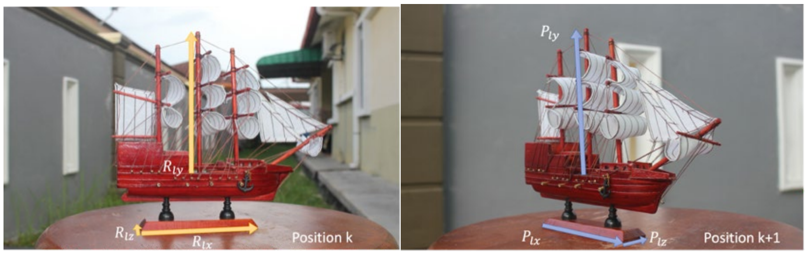

Figure 8: Camera view at (Left) k^{th} position, (Right) $k+1^{th}$ position

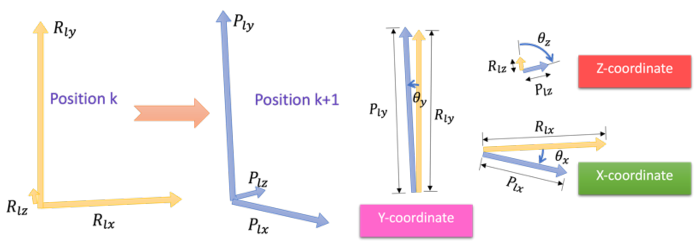

Figure 9: (Left) Illustration of the camera position at k^{th} to $k+1^{th}$ in 3D space (Right) Orientation angles obtained from the position changes plotted on 3D space

Results and Discussions

Each method's 3D scan results are presented in this section. Each strategy is thoroughly evaluated before being detailed in this section. To generate a fair and unbiased comparison analysis, each approach uses the same model.

Laser scanning method

Figures 10 and 11 show the 3D point cloud output of a sailing vessel in a room obtained using a laser scanning approach and processed in the RVIZ environment. The varying colours of the point cloud represent the distance between RPLiDAR and obstacles. The produced point cloud shows the wall and ceiling, but there is no view of the floor. A greenish-yellow point cloud represents sailing vessels, while a redpoint cloud depicts the RPLiDAR's closest impediments during scanning. The violet point cloud in Figures 10 and 11 strongly resembles the sailing vessel in the greenish-yellow point cloud. To summarise, the RPLiDAR successfully scanned a traditional sailing sailboat in the form of a point cloud, although it still requires modification in order to obtain data with higher accuracy and exact measurements.

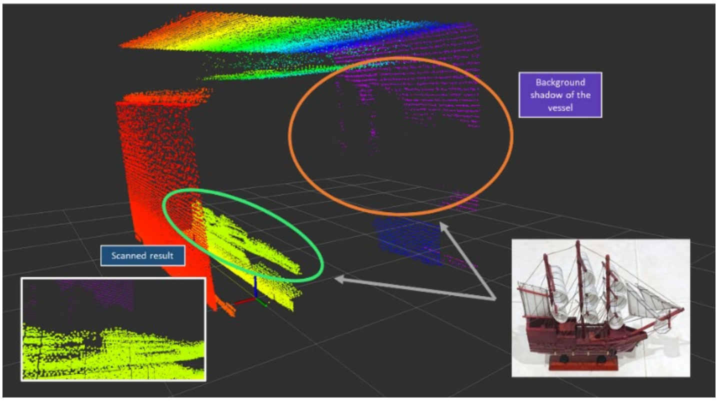

Figure 10: A view of 3D point cloud output of the sailing vessel model via RVIZ

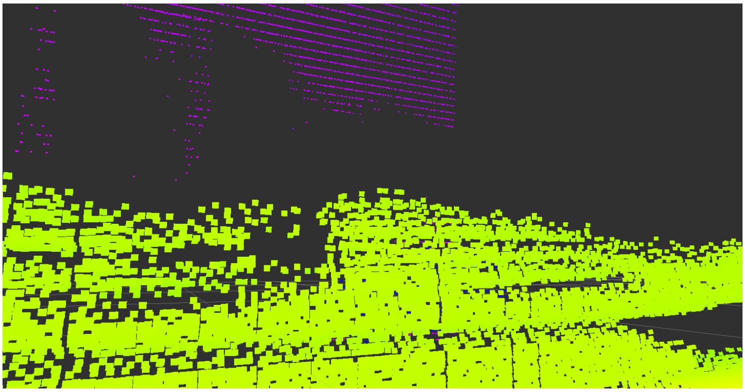

Figure 11: A closer look of the vessel point cloud

Depth Image method

The Kinect V2 depth camera is used in the evaluation experiment for the depth image approach. Figure 12 depicts the outcome.

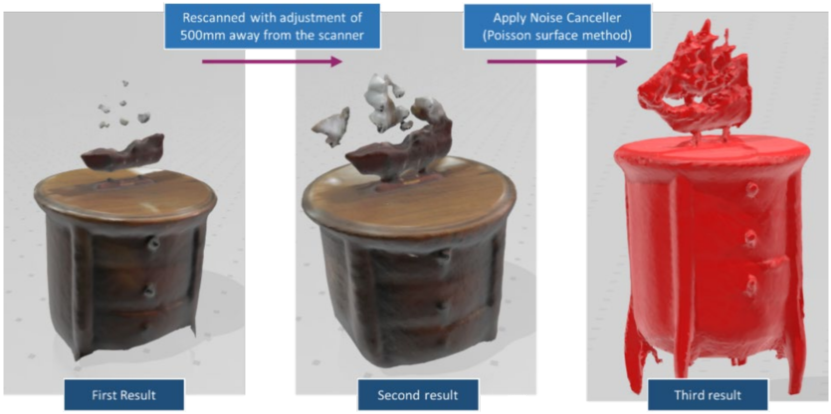

Figure 12: Workflow overview for the 3D scan using Kinect V2

Figure 12 shows the model being scanned with the Kinect V2 sensor while it is stationary on top of a small round table. The complete scan with a distance parameter of 800 mm between the Kinect and the model is the first result displayed. The Kinect was then rescanned at a closer distance to the model for the second result, with a distance of roughly 500 mm between them. Finally, the model was thoroughly re-examined, and the noise canceller was used to create a superior 3D model. Overall, the 3D model created by Kinect V2 is significantly superior to the initial technique. Despite this, the data's quality, accuracy, and precision are poor, and they can't be used to construct anything.

Photogrammetry method

To ensure that all the model's features were caught, a total of 148 photographs were taken from various perspectives. In addition, to optimise the output of the 3D model after rendering, the alignment and sequence of pictures are rigorously prepared and sorted out. The photos were captured using an anti-clockwise rotation of a circular photography approach in this case. The output of a 3D reconstruction model utilising Reality Capture is shown in Figure 13.

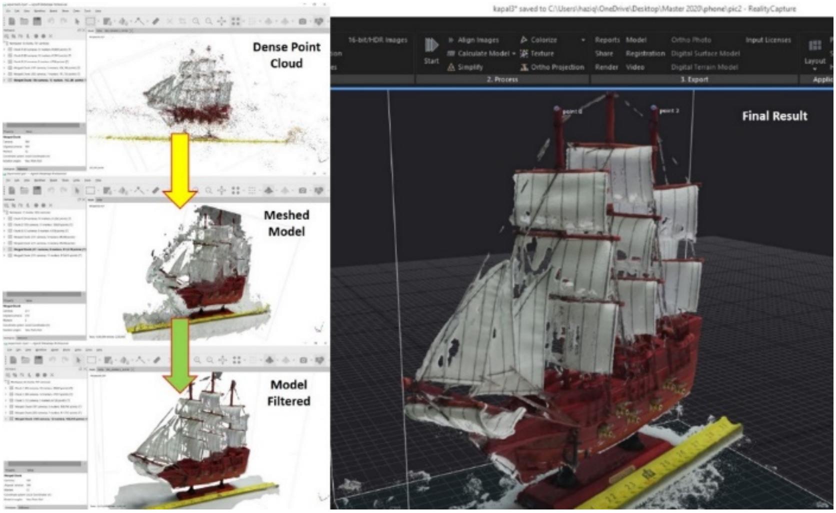

Figure 13: 3D ship model result generated by Reality Capture software

The acquired photographs go through a number of steps to get the final outcome illustrated in Figure 13. To match the correct position of imported photos, a method known as scale-invariant feature transform (SIFT) is used first, as shown in Figure 14. SIFT is a computer vision feature detection algorithm that detects and describes local features in images before matching the neighbouring images to create a proper 3D model. The SFM software can construct dense point clouds using this method by drawing gradient lines on the image and labelling the directions using feature point localization from the image's pixels. It has been demonstrated to be useful in a variety of applications such as object detection, robotic mapping and navigation, picture stitching, 3D modelling, gesture recognition, video tracking, and so on [19]. To generate a good 3D model, the point cloud is then subjected to a meshing procedure, which is followed by a texture projection step. Depending on the amount of computing power and resources available, these procedures can take a long time to perform. The completed 3D model will be sent to a Computer-Aided Design (CAD) software, such as CATIA, for model finetuning, record keeping, and blueprint preparation at the conclusion of the method.

Figure 14: The captured images are aligned according to SIFT algorithm

Analysis of model confidence level

As illustrated in Figure 15, a comparison study is performed between the physical model, the photogrammetric point cloud, and a mesh model that has been coloured according to the absolute deviation in %, one on the port (left) side and the other on the starboard (right) side. As shown in the model, the blue shaded colour represents the ideal value, which is approximately 80% to 100% confidence in measurements between the real object and the 3D model, followed by the cyan colour with 10% confidence, the green colour with 5% confidence, and the red shaded colour with an estimated measurement of only 1% to become the true model. The bigger the number of percentage values, the more accurate the authentic model will be. On the right side of the model and at the bottom of the sailcloth, the majority of the red-hued colours may be located. This could be due to the overwhelming amount of light and shadow made during the picture session, which took place in the afternoon at an open space region with dreary weather [20]. As a result, some surface portions are obliterated and covered by shadows, resulting in an estimation mistake. Furthermore, during the photo shooting process, light penetrates through the thin white sailcloth, making it appear transparent. As a result of the translucent item, the percentage of accuracy during the alignment of images will be greatly reduced, resulting in the estimation of inaccurate values. Point markers were utilised to enable the SFM algorithm in detecting the model's landmark placements in each image, as well as its orientations and depths, in order to minimise percentage errors, as illustrated in Figure 16. In this scenario, the image alignment focuses on three critical points: 1, 2, and 3, which serve as the ultimate reference for the SIFT alignment. The system's confidence grows as more reference points are added. There is a trade-off, however, between calculating time and the level of confidence in the results.

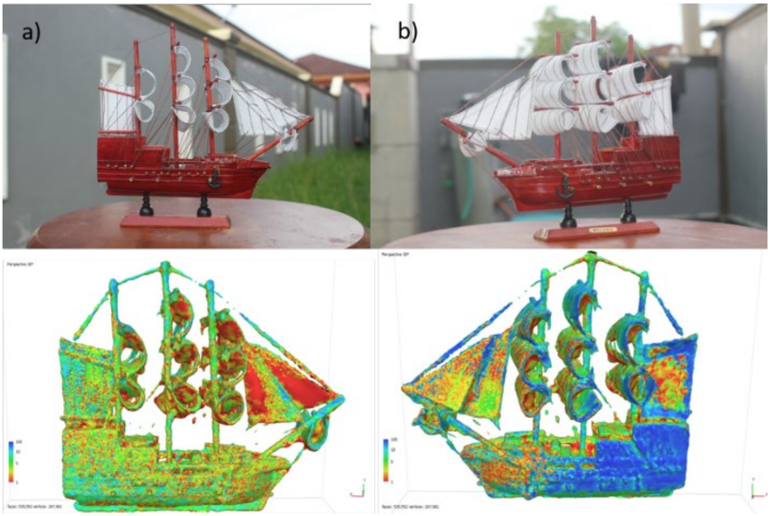

Figure 15: A comparison of the photogrammetric point cloud and mesh model coloured according to absolute deviation in percentage, a) starboard side b) port side

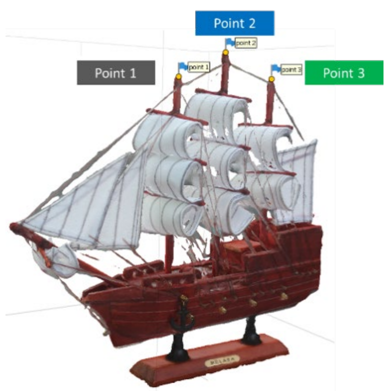

Figure 16: The alignment of images is focused on marked points using SIFT algorithm to increase confidence level

Model precision analysis

After the photos have been aligned, a polygonal model (structured data) is created, followed by texture synthesis to produce the most realistic digital representation of the physical model possible. To improve the status of the reconstructed 3D model, a second round of fine-tuning was performed on the produced model. To show that this method is effective for use as a preservation and recording documentation method for objects, it is important to analyse and compare the 3D model dimensions to the real dimensions of a physical model.

Several points on the rebuilt 3D model have been highlighted to make studying model precision easier, as illustrated in Figure 17. The Sailcloth holder length (pt. 1 to pt. 2), Base Width (pt. 3 to pt. 4), Bowsprit length (pt. 5 to pt. 6), and Base length (pt. 5 to pt. 6) have all been identified as potential precision analysis possibilities (pt. 7 to pt. 8)

Table 1 displays tabulated statistics for % inaccuracy on selected areas of physical and 3D reconstructed models, identical to Figures 18 and 19. According to the measurement, the Base length has the lowest percentage inaccuracy, which is 0.83 percent. The bowsprit length, on the other hand, has the highest percentage inaccuracy at 2.40 percent of the entire length. Most of the time, the percentage of inaccuracy is around 1.6125 percent of the total. According to the percentage error numbers shown in the table, photogrammetry technology combined with SFM software can rebuild a high-quality and precise 3D model. As a result, the percentage of accuracy can be calculated by subtracting the greatest percentage error, 2.40 percent, from 100 percent and getting 97.6 percent.

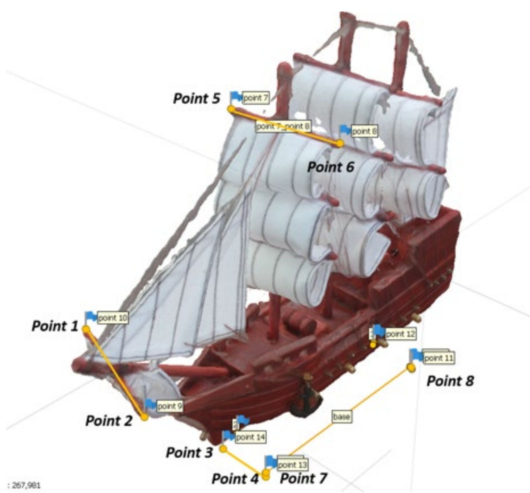

Figure 17: Marked points on the reconstructed 3D model to facilitate precision analysis

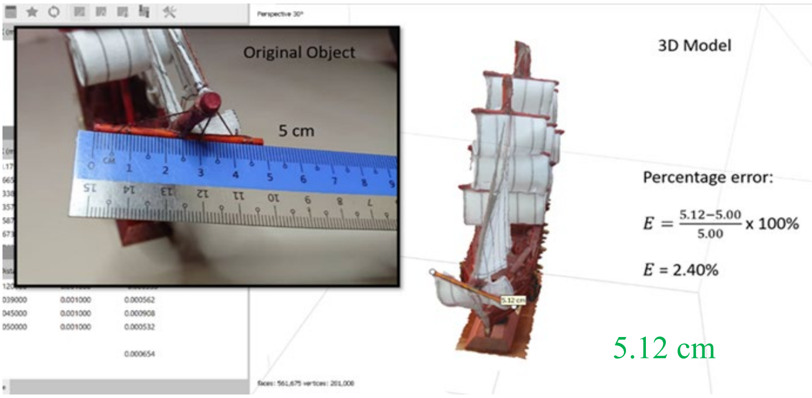

Figure 18: Dimension accuracy of the selected sections of the reconstructed 3D model

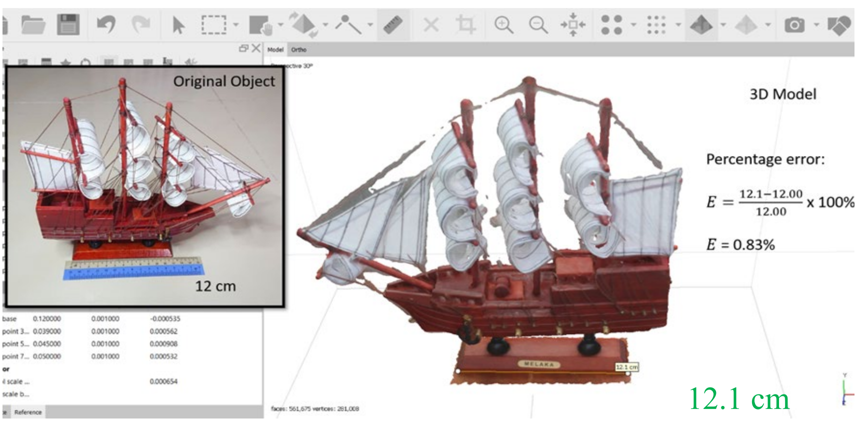

Figure 19: Dimension accuracy of the selected sections of the reconstructed 3D model

Table 1: Percentage error between physical and 3D reconstructed models

Part	**Actual Dimension**	**Model Dimension**	**% Error**
Sailcloth holder length	5.00cm	5.11cm	2.20
Bowsprit length	5.00cm	5.12cm	2.40
Base length	12.00cm	12.10cm	0.83
Base Width	3.00cm	3.05cm	1.02

SFM software performance: reality capture vs Agisoft metashape

A total of 148 pictures were recorded and imported into two different processing platforms, Reality Capture and Agisoft Metashape software, to create the final output for the model of "Flor de la Mar." When it comes to processing speed, Metashape is outperformed by Reality Capture. Metashape takes an average of 154 minutes, or nearly three hours, to complete all of the processes required to recreate the 3D model. Reality Capture, on the other hand, processes data in a fraction of the time it takes Metashape, taking an average of 74 minutes (about one hour) with identical settings and installations. As seen in Figure 20, Reality Capture surpasses Metashape in terms of output quality, delivering more details and fewer open holes than Metashape.

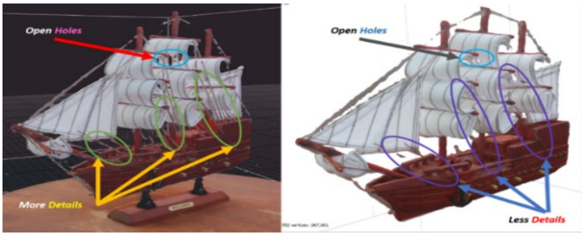

Figure 20: The comparison output result between Reality Capture (left) and Metashape (right)

Orthographic projection compilation

Finally, as illustrated in Figure 21, the successful 3D model is projected into an orthographic view for a basic documentation record. In terms of reconstruction quality, accuracy, and precision, the photogrammetry approach exceeds both laser and depth camera methods, as evidenced by a comprehensive study output.

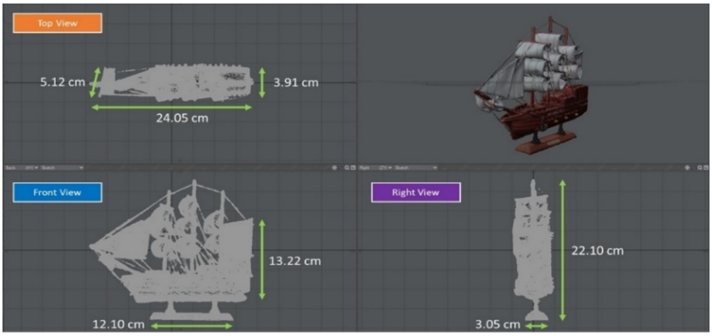

Figure 21: The orthographic projection of the “Flor de la Mar” model

Conclusion

This research examines the ability of laser scanning, depth camera, and photogrammetry approaches to aid in the digital reconstruction of three-dimensional (3D) models. According to the data, laser scanning is the least preferable approach for reconstructing a 3D model. The results of an experiment carried out using RPLiDAR A2M8 reveal that it is only capable of generating point clouds and is unable to construct 3D models. The 3D model created using the depth camera method is fairly rudimentary, with few surface details and warped portions. Kinect sensors, on the other hand, are light-sensitive and have a limited scanning area. The photogrammetry approach gives a good result with great precision in dimensions and excellent quality in 3D texture. This achievement will aid in the preservation of national heritages in the augmented reality environment, as well as provide a more realistic approach of developing future form design blueprints.

In terms of SFM software, i.e., photogrammetry post-processing Reality Capture software exceeds Agisoft Metashape in two important areas: processing speed and output quality. Using the ship model as a test model, Reality Capture software can scale the model back to its original size, which is 1:1 scaled with precision and has a 97.6% of accuracy.

Acknowledgment

This work is supported in part by Ministry of Higher Education grant Fundamental Research Grant Scheme Ref: FRGS/1/2019/WAB09/UITM/03/2.

References

[1] L. Sui and L. Lin, "Design of Household Cleaning Robot Based on Low-cost 2D LIDAR SLAM," *2020 Int. Symp. Auton. Syst. ISAS 2020*, pp. 223–227, 2020, doi: 10.1109/ISAS49493.2020.9378863.

[2] J. P. Queralta *et al.*, "FPGA-based Architecture for a Low-Cost 3D Lidar Design and Implementation from Multiple Rotating 2D Lidars with ROS," *Proc. IEEE Sensors*, vol. 2019-Octob, pp. 2019–2022, 2019, doi: 10.1109/SENSORS43011.2019.8956928.

[3] N. L. Neuta, S. A. Vivas, N. V. Fajardo, O. F. R. Giraldo, and V. R. Cano, "Low-cost recognition and classification system based on LIDAR sensors," *2018 IEEE 2nd Colomb. Conf. Robot. Autom. CCRA 2018*, pp. 3–8, 2018, doi: 10.1109/CCRA.2018.8588139.

[4] R. Siv, I. Ardiyanto, and R. Hartanto, "3D human face reconstruction using depth sensor of Kinect 2," *2018 Int. Conf. Inf. Commun. Technol.*

ICOIACT 2018, vol. 2018-January, pp. 355–359, 2018, doi: 10.1109/ICOIACT.2018.8350702.

[5] F. I. Apollonio, F. Fantini, S. Garagnani, and M. Gaiani, "A photogrammetry-based workflow for the accurate 3d construction and visualization of museums assets," *Remote Sens.*, vol. 13, no. 3, pp. 1–40, 2021, doi: 10.3390/rs13030486.

[6] X. Kang, S. Yin, and Y. Fen, "3D reconstruction assessment framework based on affordable 2D lidar," *IEEE/ASME Int. Conf. Adv. Intell. Mechatronics, AIM*, vol. 2018-July, pp. 292–297, 2018, doi: 10.1109/AIM.2018.8452242.

[7] M. R. Shahrin, F. H. Hashim, W. M. D. W. Zaki, A. Hussain, and T. Raj, "3D indoor mapping system using 2D LiDAR sensor for drones," *Int. J. Eng. Technol.*, vol. 7, no. 4, pp. 179–183, 2018, doi: 10.14419/ijet.v7i4.11.20797.

[8] J. Li, X. Zhang, J. Li, Y. Liu, and J. Wang, "Building and optimization of 3D semantic map based on Lidar and camera fusion," *Neurocomputing*, vol. 409, pp. 394–407, 2020, doi: 10.1016/j.neucom.2020.06.004.

[9] J. Li, X. He, and J. Li, "2D LiDAR and camera fusion in 3D modeling of indoor environment," *Proc. IEEE Natl. Aerosp. Electron. Conf. NAECON*, vol. 2016-March, pp. 379–383, 2016, doi: 10.1109/NAECON.2015.7443100.

[10] J. P. Virtanen, K. N. Antin, M. Kurkela, and H. Hyyppä, "The feasibility of using a low-cost depth camera for 3D scanning in mass customization," *Open Eng.*, vol. 9, no. 1, pp. 450–458, 2019, doi: 10.1515/eng-2019-0056.

[11] H. L. L. Wellens, H. Hoskens, P. Claes, A. M. Kuijpers-Jagtman, and A. Ortega-Castrillón, "Three-dimensional facial capture using a custom-built photogrammetry setup: Design, performance, and cost," *Am. J. Orthod. Dentofac. Orthop.*, vol. 158, no. 2, pp. 286–299, 2020, doi: 10.1016/j.ajodo.2020.01.016.

[12] Y. Zhang, T. Jia, Y. Chen, and Z. Tan, "A 3D Point Cloud Reconstruction Method," *9th IEEE Int. Conf. Cyber Technol. Autom. Control Intell. Syst. CYBER 2019*, pp. 1310–1315, 2019, doi: 10.1109/CYBER46603.2019.9066630.

[13] M. Samir, E. Golkar, and A. A. A. Rahni, "Comparison between the Kinect^{TM} V1 and Kinect^{TM} V2 for respiratory motion tracking," *IEEE 2015 Int. Conf. Signal Image Process. Appl. ICSIPA 2015 - Proc.*, pp. 150–155, 2016, doi: 10.1109/ICSIPA.2015.7412180.

[14] A. Tariq, S. M. O. A. Gillani, H. K. Qureshi, and I. Haneef, "Heritage preservation using aerial imagery from light weight low cost Unmanned Aerial Vehicle (UAV)," *Int. Conf. Commun. Technol. ComTech 2017*, pp. 201–205, 2017, doi: 10.1109/COMTECH.2017.8065774.

[15] I. Reljić and I. Dunder, "Application of photogrammetry in 3D scanning of physical objects," *TEM J.*, vol. 8, no. 1, pp. 94–101, 2019, doi: 10.18421/TEM81-13.

[16] R. Pacheco-Ruiz, J. Adams, and F. Pedrotti, "4D modelling of low visibility Underwater Archaeological excavations using multi-source photogrammetry in the Bulgarian Black Sea," *J. Archaeol. Sci.*, vol. 100, no. May, pp. 120–129, 2018, doi: 10.1016/j.jas.2018.10.005.

[17] H. El-Din Fawzy, "3D laser scanning and close-range photogrammetry for buildings documentation: A hybrid technique towards a better accuracy," *Alexandria Eng. J.*, vol. 58, no. 4, pp. 1191–1204, 2019, doi: 10.1016/j.aej.2019.10.003.

[18] S. Yang, W. Jiang, and B. Tian, "ISAR image matching and 3D reconstruction based on improved SIFT method," *Proc. - 2019 Int. Conf. Electron. Eng. Informatics, EEI 2019*, pp. 224–228, 2019, doi: 10.1109/EEI48997.2019.00056.

[19] H. El-Din Fawzy, "Study the accuracy of digital close range photogrammetry technique software as a measuring tool," *Alexandria Eng. J.*, vol. 58, no. 1, pp. 171–179, 2019, doi: 10.1016/j.aej.2018.04.004.

[20] R. A. Galantucci and F. Fatiguso, "Advanced damage detection techniques in historical buildings using digital photogrammetry and 3D surface anlysis," *J. Cult. Herit.*, vol. 36, pp. 51–62, 2019, doi: 10.1016/j.culher.2018.09.014.